External boundaries and internal shear bands in granular convection

James B. Knight
The James Franck Institute and the Department of Physics, The University of Chicago, Chicago, Illinois 60637
(Received 23 September 1996)

Granular material convects in response to vertical vibrations of sufficient peak acceleration. Particles flow upward in the center of a container with rough, vertical walls and downward in a thin stream along the sides. Canting the side walls outward from the vertical beyond a transition angle reverses the sense of the flow and changes its shape: particles flow upward in a broad region above the walls and downward in the center. We have studied this transition experimentally and find evidence for two opposing mechanisms, net downward shear at a rough vertical wall and ''ratcheting'' at an oblique wall, which combine to determine the effect of the boundaries on particle motion. The direction of convective flow is not solely a function of the external boundaries, however. Continuous vibration can induce internal shear bands at which the flow is always observed to move downward, in which case a competition between the internal shear and the shear at the external boundaries determines the overall pattern of convection. [S1063-651X(97)14903-0]

PACS number(s): 46.10.+z, 47.27.Te, 64.75.+g, 87.59.Pw

I. INTRODUCTION

Vertical vibrations with a peak acceleration exceeding gravity can excite convection rolls in dry, cohesionless granular material [1]. In a cylindrical or rectangular container, particles move upward in the center and return in a thin stream along the walls. The apparent fluidity of granular convection and other examples of granular motion invites continuum descriptions [2–5] but obscures fundamental differences from conventional fluid flow. Granular convection can occur in containers as small as ten particles across, whereas bulk fluid motion is typically a long wavelength average over a statistically large number of molecules. Similarly, the microscopic velocity scales in fluids arise from thermal energy, which is insignificant to the motion of macroscopic (noncolloidal) particles for which the relevant energy scale is the gravitational potential energy gained by raising a particle one diameter. Perhaps the most readily apparent difference is at the edge of granular convection: instead of the no-slip boundary condition ubiquitous to fluids [6], particle flow can be fastest at the container walls [7–9].

Nonetheless, the formulation of a comprehensive theory of granular flow, perhaps modeled on the Navier-Stokes equation for fluids, remains a primary goal in the interdisciplinary field of granular materials. Precise experimental characterization of representative granular flow phenomena such as convection plays a key role in this effort, providing ''benchmarks'' against which theory and simulation can be tested. Granular convection has several attractive features for experimental work [7–9]. While the absence of thermal and spatial averaging inevitably renders many types of granular motion noisy and difficult to reproduce, granular convection is remarkably stable. By varying the peak acceleration or the frequency of the driving vibration, the convection velocity can be changed reproducibly by orders of magnitude, opening a wide range of granular flow speeds to experimental study. Finally, the circulatory motion of convection confines the flow to a closed volume, simplifying the necessary apparatus and facilitating experiments of long duration.

Despite the attention granular convection has attracted, beginning with Faraday's initial observations [10] and continuing with modern experimental [7–9,11–18] and simulational [19–25] work, a comprehensive description has yet to be established. The flow in containers with rough, vertical walls has been extensively studied, but comparatively little is known about the motion in more general container geometries [4,9,11]. Even subtle changes in the external boundaries can dramatically affect granular convection. For example, flow speeds depend sensitively upon wall friction, and reducing the wall friction can in some cases suppress convection [7,9]. Canting the side walls outward from the vertical can induce a transition to flow downward in the center of the container and upward along the boundaries [7,11]. A description of the relationship between the external boundaries and the resulting flow patterns is a necessary precursor to a more general theoretical understanding.

In previous work, we measured the flow characteristics of granular convection in a fixed container geometry with vertical walls [7–9]. Vibrations were applied as discrete oscillations, or ''taps,'' with sufficient time between successive taps to allow the particles to come to rest. Both of these restrictions are relaxed in this paper. The container geometry was altered by varying the angle of the side walls, and the resulting flow was observed with photographic techniques, magnetic resonance imaging (MRI), and high speed video. We find that the transition angle beyond which the side walls must be rotated in order to drive flow downward in the center of the container and upward along the walls depends sensitively upon friction but not upon the vibration acceleration. This flow differs from the convection observed with vertical walls in direction and shape: particles move in a broad region above the side walls as opposed to being confined to a thin layer. Two mechanisms, shear at a rough vertical wall and ''ratcheting'' at an oblique wall, compete to determine the direction of flow at the boundaries. A departure from this behavior occurs if the vibrated bed collides with the upper surface of the container, in which case flow can reverse at a lower transition angle. We further find that the direction of the convective flow is not solely a function of wall angle. Above a threshold acceleration for period doubling in the

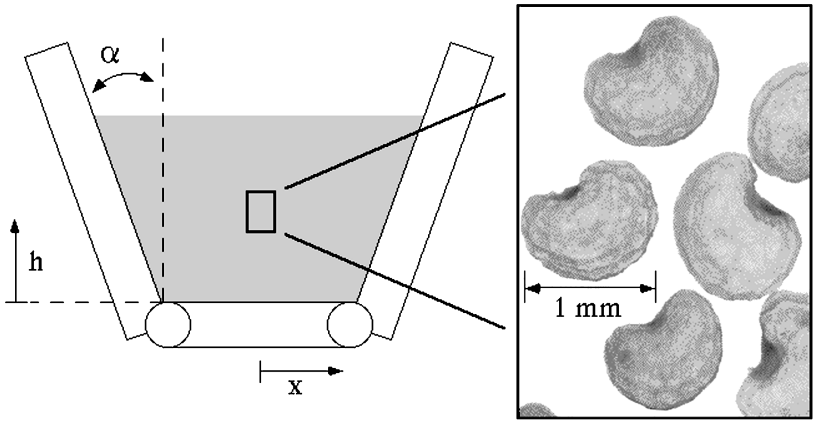

FIG. 1. (a) Schematic drawing of the apparatus. The inset is a magnified image of several poppy seeds.

flight time of a continuously vibrated bed of particles, internal shear bands can form where flow is always downward [14,26]. A competition between these internal shear bands and shear at the external boundaries determines the overall pattern of convection.

II. IMAGING THE FLOW

Figure 1 is a schematic of the container used for most of the experiments described in this paper. The side walls are separated at the bottom by a fixed base and are adjustable to any angle α from the vertical, $\alpha=0°$, up to $\alpha=45°$. The base is 52 mm wide, and the acrylic front and back plates are spaced 6 mm apart. Poppy seeds (blue and white) were added to a height of 50 mm and the entire assembly was rigidly attached to a carefully leveled electromagnetic vibration exciter. The poppy seeds were dry and elliptical in shape, with a long axis of 1 mm and a short axis of approximately 0.7 mm. The inset of Fig. 1 is a magnified image of several poppy seeds.

Both smooth and rough lateral boundaries were studied. The smooth boundaries were prepared by covering the side walls with plastic tape [27] (adhesive side against the wall), while the rough walls had a layer of poppy seeds epoxied to them. The top boundary was removed, and the container was sufficiently high to prevent particle loss during vibration. The bottom boundary was kept smooth. The acrylic front and back plates were periodically treated with an antistatic preparation [28] to prevent the accumulation of static charge. After preparation, the container was vibrated, and the resulting acceleration was monitored with an accelerometer attached to the vibration stage. We parametrize the strength of the applied acceleration by Γ, the dimensionless ratio of the peak acceleration A to that of gravity, $g=9.8$ m/s^2: $\Gamma=A/g$. The frequency of vibration f is also an important control parameter in granular convection [7]; throughout this paper, we hold it constant at $f=25$ Hz unless otherwise stated.

Figures 2(a)–2(c) are long exposure photographs of flow for three different wall angles: $\alpha=13°$, 25°, and 39°. In each case, the walls were smooth and the vibration acceleration was $\Gamma=4.2$. The container was illuminated with a strobe light repeating at the same frequency as the applied vibration (25 Hz), thereby eliminating from the photographs all motion but that of the particles. The film was exposed for about 1 s, or 25 vibration cycles, to reveal the streamlines of the flow.

The poppy seeds are airborne at the phase of the motion captured in Fig. 2. The bottom edge of the bed is flat and remains so throughout the time that the seeds are separated from the container bottom. The seeds lift off and return to the container bottom within one period of the driving oscillation. The structure of the convection in these photos differs substantially from that observed in containers with vertical boundaries, not only in that the particles move down in the center and up along the side walls, but also in that the flow along the walls is not confined to a thin layer. Instead, all of the particles above the side walls appear to move upward. The boundaries between upward and downward flow (located at the minima of the streamlines) for both 13° and 25° lie slightly interior to the corners. At 39°, this boundary curves closer to the walls near the top surface of the bed. We attribute this to the contribution of a convection roll between the front and back plates, which becomes more pronounced at high wall angles and low accelerations. The velocity of the front-to-back convection decreases rapidly with depth from the top surface.

Photography is ideal for capturing the stream lines at the front surface of a thin container, but magnetic resonance imaging provides a noninvasive probe of motion inside the container. Oil-bearing seeds contain enough free protons to produce a detectable magnetic resonance signal, and mustard and poppy seeds have been used in recent studies of granular flow in rotating drums [29] and convection in vertically shaken cylinders [8,9].

Figures 3(a) and 3(b) are spin-tagged, magnetic resonance images of a 3-mm slice through the center of an acrylic trough ($\alpha=31°$) filled to a height of 20 mm with poppy seeds. The base width (16 mm) and plate separation (18 mm) of the container are almost equal, making the container smaller in width but more three dimensional than the wide, thin geometry shown in Figs. 1 and 2. Spin tagging, described in detail elsewhere [8,9,30], entails modulating the longitudinal spin polarization in the vertical direction prior to shaking and imaging. Figure 3(a) shows a control image taken after spin tagging but without shaking. The bright regions correspond to the maxima of the spin modulation. Flow translates tagged particles, and distorts the original pattern, permitting direct measurement of the local velocities. Figure 3(b) shows the deformation after a single shake of $\Gamma=5$ and $f=20$ Hz [31]. Because of the rapid decay of the spin-tagging pattern, 256 identical shakes are necessary to obtain a single image [32], and Fig. 3(b) is an average of 4 such images.

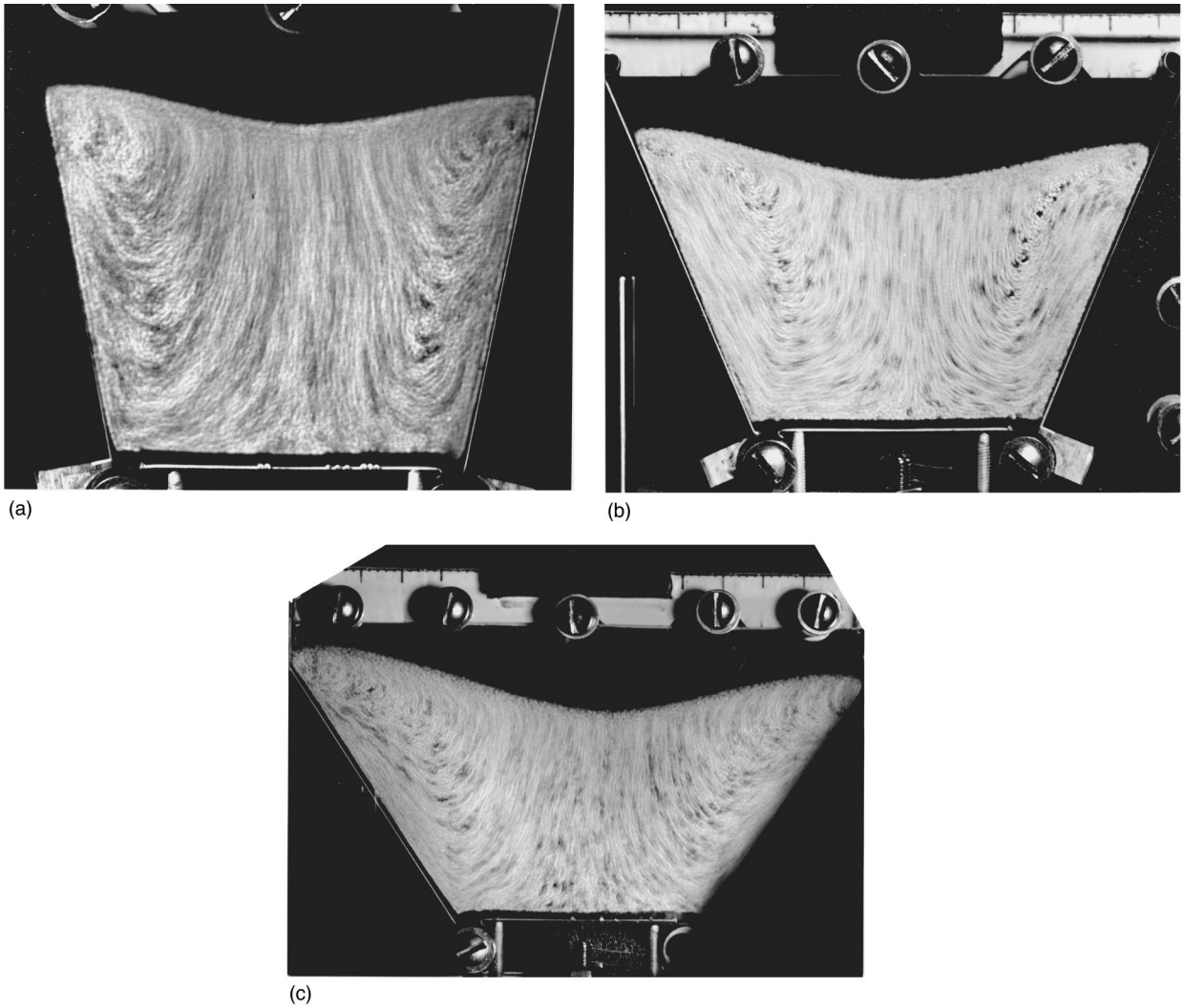

FIG. 2. Long exposure (1 s) photographs of the flow with $\Gamma=4.2$, $f=25$ Hz, and (a) $\alpha=13°$, (b) $\alpha=25°$, and (c) $\alpha=39°$. The container is 52 mm wide at the base and the front and back plates are separated by 6 mm. Flow is down in the center and up along the walls. Illumination was provided by a strobe synchronized to the vibrations of the container.

Figure 4 shows the peak positions of the flow lines (solid lines) extracted from the image in Fig. 3(b). The dotted lines represent the unperturbed position of the stripes [33]. The vertical axis is the height above the container bottom and the horizontal axis the distance from the container center. Similar measurements have been made in vertical cylinders and can be compared with Fig. 4 [8,9]. The magnitude of the velocity decreases with depth below the top surface of the bed, as it does in cylinders. In contrast to the cylindrical geometry, however, the flow lines do not appear blunted in the center, and the width of the upward flow at the walls increases with height.

III. THE TRANSITION ANGLE

MRI is an ideal tool for studying relatively fast flow in small containers. Velocity resolution and container size are limited, however, by the mechanical restrictions of vibrating the material *in situ* and by the magnetic response of the seeds [9,32]. The transition from the convective flow observed in containers with vertical walls to the reverse flow captured in Figs. 2 and 3 is not time dependent; the flow is determined entirely by boundary properties. We used the container pictured in Fig. 2 to characterize this dependence precisely by varying the angle and frictional properties of the side walls. Individual particles visible against the front plate were tracked to measure the flow velocity. This method afforded greater sensitivity to slow velocities and more range in container size than was possible with MRI.

Figure 5 shows the average vertical velocity in the center of the convective flow, $V_h(x=0)$, as a function of wall angle for smooth and rough walls. The frequency was again held constant at 25 Hz and $\Gamma=4.2$. The average velocity was measured by tracking individual particles between $h=15$ and 35 mm above the container bottom in the center of the convective flow. Positive values correspond to flow up in the middle of the container, and negative to flow down; the velocity is reported in units of distance traveled (mm) per vibration cycle. Each point is the average of at least 10 separate particles. As pictured in Fig. 2, the convection rolls were symmetric about the center of the container and the bottom interface of the particles exhibited no deformation.

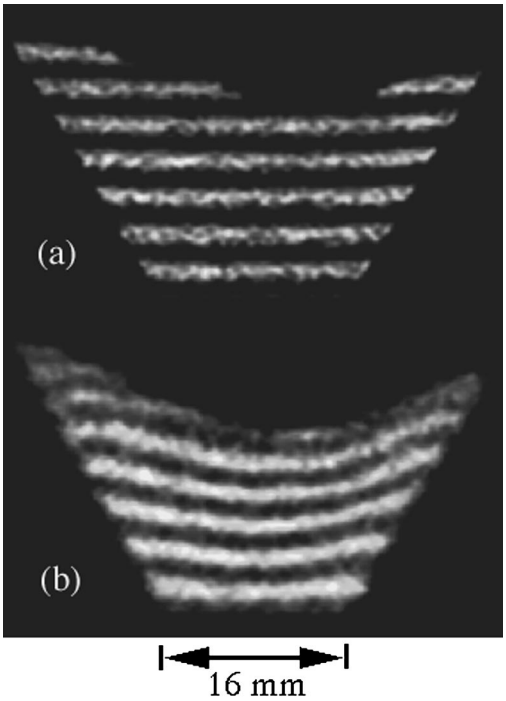

FIG. 3. Magnetic resonance images showing (a) a horizontal spin-tagging pattern before vibration, and (b) the deformation of a horizontal spin-tagging pattern after a single shake of $\Gamma=5$ and $f=20$ Hz.

At low angles (nearly vertical), flow is up in the center and down along the walls. The average vertical velocity decreases smoothly with increasing wall angle through an angle α_c, above which the flow changes direction and moves down in the middle and up along the walls. This transition angle is a function of wall friction: $\alpha_c \approx 3°$ for smooth walls (tape) and $\alpha_c \approx 10°$ for rough walls (glued seeds). The magnitude of $V_h(x=0)$ above α_c is larger for the smooth walls up to $\alpha \approx 25°$, at which point the velocities for both extremes of friction converge. The flow speed in the low friction case reaches a maximum in magnitude between 10° and 15°. The top surface of the convecting bed is highest in the center and slopes downward toward the walls at angles below α_c. Above the transition, at angles $\alpha > \alpha_c$, this heap profile inverts so that the top surface is lowest in the center of the container and slopes up towards the walls (see Fig. 2). The top surface is flat near α_c.

We did not observe an acceleration dependence to α_c.

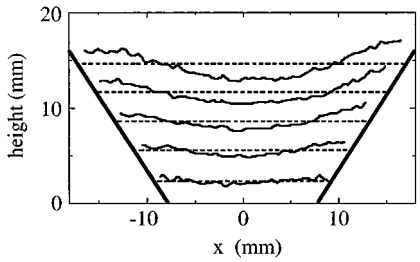

FIG. 4. The peak positions of the spin-tagging stripes in Fig. 3(b). The dotted lines represent the unperturbed position of the stripes, and span the width of the container. The angled container walls are shown as thick, diagonal lines.

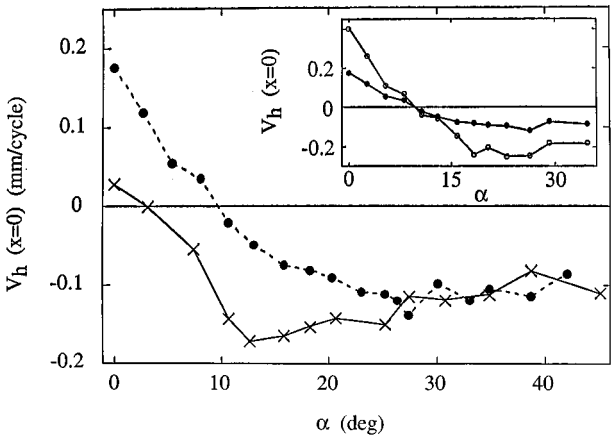

FIG. 5. Average velocity in the center of the convective flow, $V_h(x=0)$, plotted against the wall angle α for smooth (×) and rough (●) boundary conditions. The vibration parameters are $\Gamma=4.2$ and $f=25$ Hz. The data are connected by lines for clarity. The inset shows the same measurement with rough walls for two accelerations: $\Gamma=4.2$ (●) and $\Gamma=5.6$ (○). A solid line is drawn through $V_h(x=0)=0$ in both graphs.

The inset of Fig. 5 is a plot of $V_h(x=0)$ as a function of α for rough walls at $\Gamma=4.2$ and $\Gamma=5.6$. Both curves intersect zero at $\alpha_c \approx 10°$. The convective flow is faster at the higher acceleration both above and below α_c, and the two curves can be scaled onto one another by a multiplicative factor.

At sufficiently high accelerations, a vibrated bed of particles can no longer lift off of the container bottom and return within a single period of the driving vibration. Instead, a more complex motion (which will be discussed in detail below) arises that repeats over two periods of the vibration. In order to isolate the acceleration dependence of α_c at high accelerations in the absence of this ''period doubling'' transition, we vibrated the container in Fig. 1 with discrete, vertical shakes (''taps'') separated by a waiting period long enough to allow complete relaxation of the material between taps. Instead of poppy seeds, 2-mm glass beads were used to facilitate easier tracking through the taps. Measurements of the convective velocity as a function of wall angle and roughness yielded results equivalent to those shown in Fig. 5. The wall angle was then adjusted to a value just below α_c and the acceleration was increased. Flow remained up in the center of the container and down along the sides over the entire range of acceleration accessible with our equipment ($\Gamma<15$).

Top boundary. If the particles collided *en masse* with the container lid roll reversal could occur even at $\alpha<\alpha_c$. We tested this with both a solid lid and a wire mesh top (spaced to stop particles but allow air passage) to the same effect. Roll reversal through collision with the top boundary has not been studied with vertical walls [33].

IV. INTERNAL SHEAR BANDS

A period doubling bifurcation in the flight time of a vibrated bed of granular material was first identified by Douady *et al.* [26]. At low vibration accelerations, larger than gravity but below a threshold value for bifurcation Γ_b, the bed lifts off of the container floor and returns with a

single flight time τ_f. This motion is repeated at the same frequency as that of the applied vibration, and τ_f is less than the period of the applied vibration T. Above Γ_b, the bed alternates between a flight time longer than T, τ_f^L, and one shorter than T, τ_f^S. This cycle repeats itself at half the driving frequency and is therefore identified as ''period doubling'' [14,26]. Even more flight times are introduced at higher accelerations. A similar transition occurs for an inelastic ball bouncing on a vibrating table, with the exception that in granular beds Γ_b is increased by dissipative processes such as air drag and by increasing bed height [26].

While the chaotic dynamics of a bouncing ball are the subject of recent work [34], the importance of this period doubling transition to granular dynamics stems from the pattern formation [35] and flow [14,17,26] associated with it. Unlike an inelastic ball, a bed of granular material is not held together by attractive forces, and above Γ_b regions within the bed can move out of phase with one another. One region may be on the long flight described by τ_f^L, while its neighbors complete the short flight τ_f^S. This decoupling in phase leads to a deformation in the bottom boundary of the vibrated bed [26].

Previous authors have called the boundary between regions vibrating out of phase with one another a defect [26] or node [14]. We observe, in agreement with past work, that the time averaged flow at such a boundary is always downward, and attribute this to a net downward shear between the regions moving in opposition (see below). We therefore propose the term ''internal shear band'' as more descriptive and less ambiguous than other names. Unlike the time averaged flow, the instantaneous particle velocities at an internal shear band are not always directed downward, as the shear band is formed at the interface of two regions of the material moving in opposition to one another. The net downward flow at an internal shear band spawns convection rolls [14,26], and the formation of multiple shear bands leads to multiple convection rolls. Douady *et al.* have shown that while a variable number of ''nodes'' or shear bands can exist at a given acceleration, there is a maximum number that depends upon Γ and the bed height [26].

The formation of internal shear bands is hysteretic [14,26], and their absence at accelerations above Γ_b is possible (even likely in confined systems). A shear band can arise ''spontaneously,'' or be induced. For example, introducing an ersatz vertical boundary into the interior of the bed with a thin rod or air jet can form a shear band that persists even after the perturbation is removed. Internal shear bands also arise above small protuberances on the bottom surface of the container. Once formed, they persist as the acceleration is lowered, although we have not observed shear bands below Γ_b.

Figures 6(a) and 6(b) show the bottom edge of a 10-mm-high layer of poppy seeds before and after the formation of an internal shear band. The container in Fig. 1 was prepared with smooth, vertical side walls and vibrated at $\Gamma=8.4$ and $f=25$ Hz. The bed motion was recorded at 1000 frames/s using a Kodak Ektapro High Speed Video System and then analyzed frame by frame. Figure 6 shows the bottom edge of the bed at two times separated by one vibration period. The vertical axis is the height above the container bottom and the horizontal axis the distance from the container center. The phase of the measurement coincides with the minimum of the container position and the maximum separation between the seeds and the container floor. The bed motion repeats over two periods of the driving vibration. In Fig. 6(a) the top curve corresponds to the long flight time and the bottom curve to the short flight time. In both cases, the bottom edge of the bed is flat; no phase boundaries were observed throughout the entire motion.

Figure 6(b) shows the same bed after the formation of an internal shear band near the center of the container. The bottom edge of the bed is no longer flat, and the regions to either side of the shear band move out of phase with one another, their motion separated in time by one period of the driving vibration. The center of the shear band, which is the border of this opposing motion, lies at the intersection of the curves in Fig. 6(b).

The circular arrows in Fig. 6 show the direction of the time averaged flow in the bed above the interface. They are intended only to convey the number and orientation of the rolls, and not details of the flow velocities. Prior to onset, flow is down along the walls and up in the middle; this motion reverses with the formation of a shear band in the center. More generally, the flow pattern is determined by competition between flow at the wall and internal shear bands. Figure 6(b) illustrates the case of relatively low friction at the walls: flow reverses but the total number of rolls remains the same (two, one on each side of the container). With rough vertical walls in the same container, flow is always down at the walls, and the formation of a node increases the number of rolls from 2 to 4. This is shown in Fig. 6(c), which was collected under identical conditions to Fig. 6(b) but with a layer of poppy seeds glued to the walls.

In a container with walls angled to $\alpha>\alpha_c$, flow in the absence of a shear band is down in the center and up along the walls. The formation of a single shear band in the center increases the flow speeds but does not alter the flow direction. Multiple nodes can force flow in either direction along walls angled at $\alpha>\alpha_c$, but flow is always down along a rough wall angled below α_c.

Figure 7 shows the spontaneous onset of the shear band in Fig. 6(b) from the initial state in Fig. 6(a). Deformation of the bottom edge began at the right wall of the container [Fig. 7(a)]. This deformation grew and propagated towards the center of the container at a constant velocity of about 1 mm/cycle [Figs. 7(b)–7(d)]. Figure 8 shows the amplitude of the deformation, Δh, as a function of time (in units of the period of the driving vibration T). The origin of the time axis is arbitrary. As shown in the inset of Fig. 8, we define the amplitude as the difference in height between the maximum and the minimum of the bottom edge of the bed at a fixed phase of the motion; in Fig. 8 it was measured at the same phase as the dashed curves in Fig. 7. The amplitude grew faster than linearly with time, but the limited range of data prevents a more precise description of the functional form.

The curvature of the bottom edge of a vibrated bed around an internal shear band is localized to the region of shear. Figure 9 shows a single shear band produced under conditions identical to those of Fig. 6(b) but in a container more than twice as wide. Large regions of the bed are flat. The dotted lines are fits to

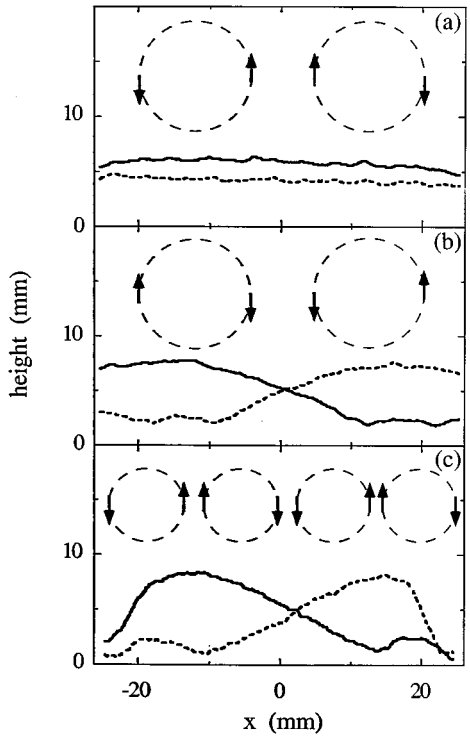

FIG. 6. Bottom edge of 10-mm-high layer of poppy seeds shaken at $\Gamma=8.4$ and $f=25$ Hz and imaged at two times separated by one shaking period. Each curve is an average over three consecutive cycles of the motion. The circular arrows above the data show the time averaged flow in the bed. (a) The minima (---) and maximum (—) of period doubling in the absence of a shear band. The container was prepared with smooth walls. (b) The same bed as in (a) after the formation of an internal shear band. (c) A single shear band in a container with rough walls. With the exception of the wall friction, the system parameters were identical to those in (a) and (b).

$$h \propto \tanh[(x-x_0)/x_c], \tag{1}$$

where x_0 is the position of the center of the shear band (close to $x=0$), and x_c the length scale of the curvature. For both curves, $x_c \approx 8$ mm, as compared to a container width of 125 mm.

V. DISCUSSION

One proposed origin of granular convection is the net downward shear that vertical walls impart to the material within [21]. This has been shown explicitly in computer simulations [21], and is consistent with experimental observations [9]. Shear depends upon three factors: wall friction, an effective pressure forcing particles against the side boundaries, and a velocity difference between the bed and the walls. Changing the angle of the walls, so that $\alpha>0$, diminishes the efficacy of this shear: particles moving upwards relative to the walls need not be in constant contact with the rough surface, even as they expand outward.

High speed video reveals a ratcheting motion at $\alpha>\alpha_c$ that leads to roll reversal. The particles lift off of the container floor during the upswing of the vibration, expand outward, and subsequently collide with the walls at a point higher than that where they started. The outer layer is pushed upwards, and the middle portion continues its slide downwards. This motion is consistent with the broad upward flow above the side walls observed in Figs. 2 and 3. The dependence of the transition angle on the wall friction is also suggested by this mechanism. Roll orientation is the outcome of a competition between the shear and ratchet mechanisms. Shear flow is favored by increasing wall friction, so α_c must increase with increasing roughness. At angles $\alpha \gg \alpha_c$, where the ratchet mechanism dominates, flow velocities are inde-

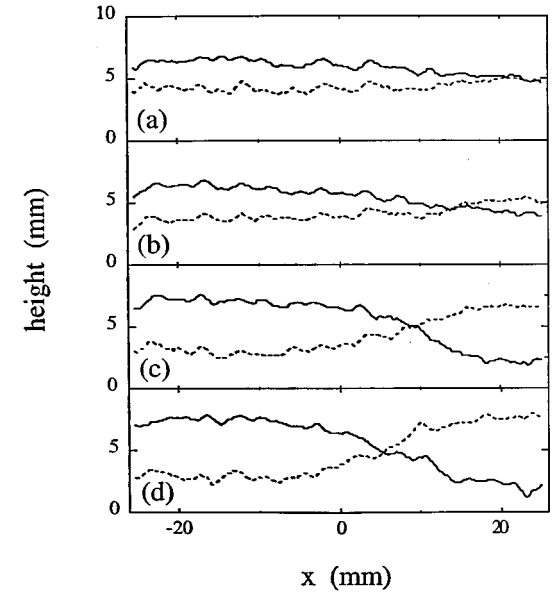

FIG. 7. (a) Onset of an internal shear band in the bed pictured in Fig. 6(a). The curves are not an average, as they are a transient state. Subsequent images taken (b) 4, (c) 8, and (d) 12 vibration periods later show the progression of the instability towards the center of the container. The final, steady state of the shear boundary is shown in Fig. 6(b).

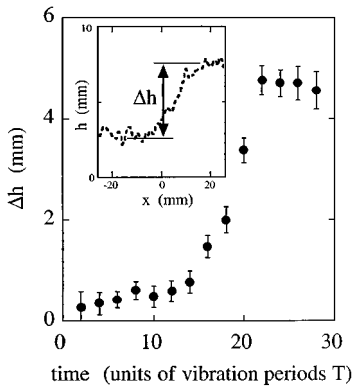

FIG. 8. Amplitude of the deformation of the bottom edge of the vibrated bed, Δh, as a function of time during the onset of the shear band shown in Fig. 7. Time is shown in units of T, the period of the driving vibration; the origin of the time axis is arbitrary. The amplitude was measured at the same phase of motion as the dashed curves in Fig. 7. The inset shows Δh for the dashed curve in Fig. 7(d).

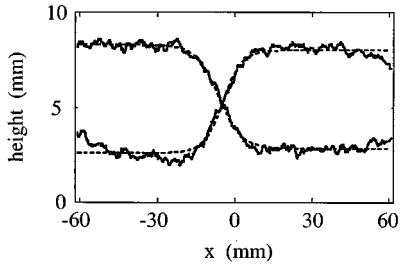

FIG. 9. Bottom edge of a 10-mm-high layer of poppy seeds shaken at $\Gamma=8.4$ and $f=25$ Hz in a thin rectangular container 125 mm wide. The plate separation is 13 mm. Figure 5 is an average over six vibration periods at times separated by one period of the applied vibration. The phase of the observation coincides with the minimum of the container motion and the maximum separation between the particles and the container. The dotted lines are fits to Eq. (1).

pendent of wall friction (Fig. 5).

Recent experiments by Aoki *et al.* [17] describe an acceleration-dependent roll reversal in containers with smooth, vertical walls. A careful evaluation of their results suggests that the transition they are in fact observing is the onset of internal shear bands. The onset acceleration they report is consistent with period doubling as is the hysteresis reported in the transition [26]. Furthermore, the images of the flow included in Ref. [17] reveal deformations in the bottom of the vibrated bed consistent with internal shear bands.

Shear arises at a vertical wall as a consequence of the difference in velocity between the airborne particle bed and the container. This is precisely the interaction that occurs between two neighboring regions of the bed at an internal shear band. Each region serves as a rough vertical wall for the other, resulting in net flow down at the shear band. This identification of a shear band as an internal rough wall is supported by several features of the data. Flow is always down at a shear band, as it is at a rough, vertical external wall. The curvature of the bed boundary is localized to the region around the shear band, and does not appear to be a global deformation of the interface (Fig. 9). Finally, an internal shear band can simply reverse the flow in a container with smooth walls [Fig. 6(b)], but not in one with walls made rough by a layer of particles [Fig. 6(c)]. In this last case the interparticle friction mediating the shear at the shear band is comparable to the wall friction, neither boundary condition prevails, and the resulting pattern spawns two additional rolls to satisfy both conditions [Fig. 6(c)]. We interpret this last situation as a competition between the downward flow induced by the node and that induced by the side walls.

The origin of internal shear bands remains obscure. Period doubling and the multiplicity of flight times that results is a necessary condition [14,26], but what feature of the system drives the bottom interface towards deformation? The gap between the bottom edge of a vibrated bed and the container floor is a measure of the potential energy of the system. The average height of the bottom edge over the one complete cycle of the period-doubled motion ($2T$), calculated from the profiles in Figs. 6(a) and 6(b), is the same before and after the formation of an internal shear band. This is physically reasonable, as the driving force is unchanged and thus the average potential energy of the system should remain constant. It is interesting to note, though, that each of the profiles in Fig. 6(b) averages independently to this same value. Through the onset of a shear band, the system evolves from alternating between a high and a low potential energy state at the peak of its motion to maintaining the same average value. The barrier to this transition is the energy dissipated at the shear band. This suggests that the onset acceleration for shear bands (and their attendant convection rolls) should increase with bed height and number, which has been observed experimentally [17].

VI. CONCLUSIONS

In the absence of internal shear bands, particle motion at the container walls during granular convection depends upon the external boundaries. Convection in a container with rough, vertical walls is driven by downward shear at the boundaries: particles flow upward in the center and downward along the walls. Canting the side walls outward introduces a ratchet mechanism that opposes this downward shear. Above a transition angle α_c, flow reverses: particles move upward along the walls and downward in the center. This convection differs not only in its sense of rotation but also in its structure. In contrast to the thin stream of particles observed moving down beside a rough vertical wall, all of the particles in the triangular wedge above the angled side walls move upward. The transition angle increases with the roughness of the wall friction while remaining independent of the vibration acceleration. If the vibrated bed collides with the container lid, however, roll reversal can occur at angles less than α_c.

Internal shear bands can form when the bed is vibrated with sufficient acceleration to induce a period doubling transition in the bed motion. Flow at a shear band is always downward, and in this sense the internal shear bands function effectively as rough, vertical walls placed within the material. The downward flow at the shear bands competes with the shear imposed by the external boundaries to determine the overall flow pattern. This can lead to upward flow even at vertical walls if the wall friction is significantly less than the interparticle friction.

ACKNOWLEDGMENTS

We wish to thank S. Nagel, H. Jaeger, E. Ehrichs, T. Metcalf, G. Karczmar, D. Kovar, E. Grossman, and M. Brenner for enlightening discussions and suggestions. MRI access was provided by M. Lipton and the University of Chicago Magnetic Resonance Imaging and Spectroscopy Facility, and the Kodak Ektapro fast imaging system was loaned to us by M. Hale and her colleagues in the biomechanics group at the University of Chicago. This work is supported in part by the MRSEC program of the National Science Foundation under Contract No. DMR-9400379. We acknowledge additional support through DOE Grant No. DE-FG02-92ER25119.

[1] For reviews of granular convection and the physics of granular materials in general, see H. M. Jaeger and S. R. Nagel, Science **255**, 1523 (1992); R. P. Behringer, Nonlin. Sci. Today **3**, 1 (1993); H. M. Jaeger, J. B. Knight, C.-H. Liu, and S. R. Nagel, Mat. Res. Bull. **19**, 25 (1994); H. Hayakawa, H. Nishimori, S. Sasa, and Y.-H. Taguchi, Jpn. J. Appl. Phys. **34**, 397 (1995); H. M. Jaeger, R. P. Behringer, and S. R. Nagel, Rev. Mod. Phys. **68**, 1259 (1996).

[2] P. K. Haff, J. Fluid Mech. **134**, 401 (1983); J. Rheol. **30**, 931 (1986); in *Granular Matter*, edited by A. Mehta (Springer-Verlag, New York, 1993), pp. 141–160.

[3] S. B. Savage, J. Fluid Mech. **194**, 457 (1988).

[4] M. Bourzutschky and J. Miller, Phys. Rev. Lett. **74**, 2216 (1995).

[5] H. Hayakawa, S. Yue, and D. C. Hong, Phys. Rev. Lett. **75**, 2328 (1995).

[6] D. J. Tritton, *Physical Fluid Dynamics* (Oxford, New York, 1988), p. 63.

[7] J. B. Knight, H. M. Jaeger, and S. R. Nagel, Phys. Rev. Lett. **70**, 3728 (1993).

[8] E. E. Ehrichs, H. M. Jaeger, G. S. Karczmar, J. B. Knight, V. Yu. Kuperman, and S. R. Nagel, Science **267**, 1632 (1995).

[9] J. B. Knight, E. E. Ehrichs, V. Yu. Kuperman, J. K. Flint, H. M. Jaeger, and S. R. Nagel, Phys. Rev. E **54**, 5726 (1996).

[10] M. Faraday, Philos. Trans. R. Soc. London **52**, 299 (1831).

[11] H. Takahashi, A. Suzuki, and T. Tanaka, Powder Technol. **2**, 65 (1968/69).

[12] G. Ratkai, Powder Technol. **15**, 187 (1976).

[13] C. F. Harwood, Powder Technol. **16**, 51 (1977).

[14] C. R. Wassgren, C. E. Brennen, and M. L. Hunt, J. Appl. Mech. **63**, 712 (1996).

[15] E. Clement and J. Rajchenbach, Phys. Rev. Lett. **69**, 1189 (1992); J. Duran, T. Mazozi, E. Clement, and J. Rajchenbach, Phys. Rev. E **50**, 3092 (1994); **50**, 5138 (1994).

[16] P. Evesque and J. Rajchenbach, Phys. Rev. Lett. **62**, 44 (1989); C. Laroche, S. Douady, and S. Fauve, J. Phys. (Paris) **50**, 699 (1989).

[17] K. M. Aoki, T. Akiyama, Y. Maki, and T. Watanabe, Phys. Rev. E **54**, 874 (1996).

[18] H. K. Pak, E. Van Doorn, and R. P. Behringer, Phys. Rev. Lett. **74**, 4643 (1995).

[19] H. J. Herrman, Physica A **191**, 263 (1992).

[20] J. A. C. Gallas, H. J. Herrmann, and S. Sokolowski, Phys. Rev. Lett. **69**, 1371 (1992).

[21] J. Lee, J. Phys. A **27**, L257 (1994).

[22] Y.-h. Taguchi, Phys. Rev. Lett. **69**, 1367 (1992).

[23] P. A. Thompson, in *Computer Simulation Studies in Condensed Matter Physics VI*, edited by D. P. Landau, K. K. Mon, and H.-B. Schüttler, (Springer-Verlag, Berlin, 1993), pp. 31–45.

[24] S. Luding, E. Clement, A. Blumen, J. Rajchenbach, and J. Duran, Phys. Rev. E **50**, R1762 (1994).

[25] T. Pöschel and H. J. Herrmann, Europhys. Lett. **29**, 123 (1995).

[26] S. Douady, S. Fauve, and C. Laroche, Europhys. Lett. **8**, 621 (1989).

[27] 3M Scotch yellow electrical tape.

[28] Tech Spray Anti-Stat.

[29] M. Nakagawa, S. A. Altobelli, A. Caprihan, E. Fukushima, and E.-K. Jeong, Exp. Fluids **16**, **54** (1993).

[30] L. Axel and L. Dougherty, Radiology **171**, 841 (1989); V. Yu. Kuperman, E. E. Ehrichs, H. M. Jaeger, and G. S. Karczmar, Rev. Sci. Instrum. **66**, 4350 (1995).

[31] The shaking method used in the MRI experiments was limited to frequencies close to 20 Hz.

[32] The spin-tagging pattern decays with a time constant of approximately 200 ms (the spin-lattice relaxation time). During this time, the seeds must be spin tagged, shaken, and imaged.

[33] The control lines have been calculated from the flow lines with the restraint that the net flow at any depth must be zero.

[34] A. Mehta and J. M. Luck, Phys. Rev. Lett. **65**, 393 (1990).

[35] F. Melo, P. Umbanhowar, and H. L. Swinney, Phys. Rev. Lett. **72**, 172 (1993); *ibid*. **75**, 3838 (1995); P. Umbanhowar, F. Melo, and H. L. Swinney, Nature **382**, 793 (1996).